Rheo-optical studies on the deformation mechanism of semicrystalline polymers. 1. Deformation mechanism and recoverability of deformation of tubular extruded polybutene-1 films

Takeji Hashimoto, Akira Todo*, Yasuhisa Tsukahara, and Hiromichi Kawai
Department of Polymer Chemistry, Faculty of Engineering, Kyoto University, Kyoto 606, Japan
(Received 10 April 1978; revised 19 September 1978)

Rheo-optical studies (involving small-angle X-ray and light scattering, wide-angle X-ray diffraction, and birefringence studies) have been applied to polybutene-1 films prepared by tubular extrusion (the preparation involving crystallization from oriented melts) to investigate the fundamental orientation and deformation mechanisms of molecules (in the crystalline and amorphous regions) and crystalline supermolecular structure. It is shown that the molecular orientation behaviour can be described by deformation of the 'row-nucleated' sheaf-like crystalline superstructure and that the deformation of the interlamellar spacing is quite uniform, the microscopic strain being identical to the strain in bulk specimens. The latter is quite important in understanding apparent 'springy' or 'hard-elastic' properties of the films observed at temperatures above the glass transition of the films. In relation to the springy properties, recoverabilities of the molecular and supermolecular structures from large extensions have been also studied.

INTRODUCTION

Rheo-optical methods have been developed to investigate the mechanical relaxation and dispersion behaviour of semicrystalline polymers in terms of the relaxation and dispersion of fundamental structural units of polymers[1-5]. Techniques such as dynamic birefringence, X-ray diffraction, infra-red absorption and light scattering have been applied to polyolefin films having a spherulitic crystalline superstructure and have provided evidence which clarifies the structural origin of α-mechanical relaxation. In the case of polyethylene, the α-relaxation seems to be composed of two superposed relaxation mechanisms: the α_1-relaxation (the lower temperature α-relaxation) and the α_2-relaxation (the higher temperature α-relaxation)[6]. We conclude that the α_1-relaxation is related to the orientation of crystallites, while the α_2-relaxation is associated with molecular motion within the crystals.

The earlier rheo-optical on the α-relaxation of polyolefins as well as our earlier papers of this series[7-11] have been applied to the films crystallized from isotropic melts (which have spherulitic crystalline superstructure). The deformation behaviour of the spherulite and its time-dependence are locally different: for example, the time-dependent deformation behaviour of the polar part of the spherulite (i.e., the part of spherulite parallel to the stretching direction) is significantly different from the equatorial part[2]. The responses of individual structural elements in the different parts of the spherulites to the applied mechanical excitation, however, tend to be evened out by the orientation distribution of the structural elements. Thus in most of the cases the rheo-optical properties cannot directly reduce the fundamental structural responses without the aid of sophisticated model calculations.

In order to study the fundamental structural responses more directly and to circumvent difficulties associated with the model calculations, we have applied the rheo-optical techniques to the crystalline superstructure developed by crystallization from oriented melts[12]. The films have 'row-nucleated' cylindrites or sheaves in which the stacks of lamellar crystals are highly oriented with their normals parallel to a particular direction (extrusion or machine direction). The evening out of the structural response due to the lamellar orientation distribution should be greatly reduced in such oriented systems, thus facilitating the studies of the structural responses. The information obtained on the oriented systems may be fed back for better understanding of the structural responses in the spherulitic systems.

It is our purpose in this article to study deformation behaviour and recoverability of deformation of the 'row-nucleated' sheaf-like superstructure at microscopic, submicroscopic and molecular levels by using various rheo-optical techniques such as light scattering, small-angle X-ray scattering, wide-angle X-ray diffraction, and birefringence. During the course of such studies, the films were discovered to exhibit apparently unique mechanical properties of so called 'hard-elasticity[13-16] or 'springy properties'[17], i.e. the films exhibiting a high degree of length recovery from large extensions, a marked reduction of apparent density, etc. Thus the

* Present address: The Research Center, Mitsui Petrochemical Industries Ltd., Waki-cho, Kuga-gun, Yamaguchi-ken, Japan

0032-3861/79/050636-13$02.00

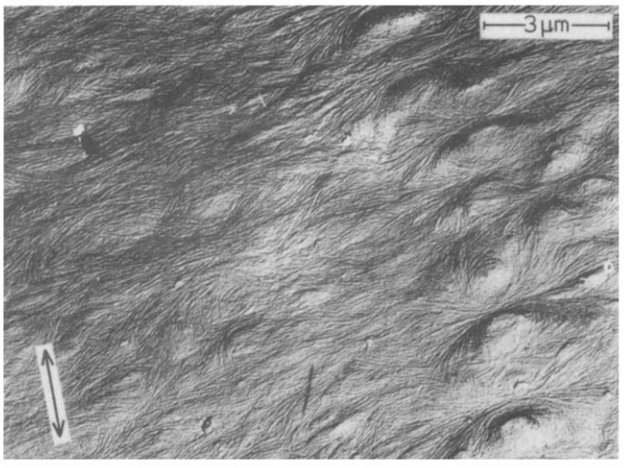

Figure 1 Typical electron micrograph of surface replicas of the specimen. Arrow indicates the extrusion direction

rheo-optical studies are inevitably connected with the studies of the apparent springy properties of the polybutene-1 films.

In this article our studies are focussed on the deformation behaviour and recoverability of the deformation of the sheaf-like superstructure and its internal lamellar stacks and on the orientation behaviour of the crystals and its recoverability, as well. The orientation behaviour of chain molecules in the amorphous phase will be discussed in detail in a subsequent paper of this series[18]. The analysis of the amorphous chain orientation is also important for a complete characterization of the deformation behaviour of the systems having a two-phase structure. The analysis, however, involves separation of the birefringence arising from amorphous chain orientation from that due to crystal orientation and form birefringence. The form birefringence contribution turned out to be extraordinarily large and its reduction from the total birefringence to be essential for an estimation of the birefringence arising from amorphous chain orientation[18].

The deformation behaviour of the superstructure and the molecular orientation behaviour thus analysed in this paper and in a subsequent paper[18] will be utilized for a better understanding of dynamic mechanical properties, dynamic birefringence, and dynamic wide-angle X-ray diffraction[19].

TEST SPECIMENS: SUPERSTRUCTURE AND MECHANICAL PROPERTIES

Pellets of polybutene-1 (Vestolen BTX1810 natural 201, Hüls, Germany) were melted at 185°C and then tubular-extruded under ordinary conditions. The films thus prepared are in the stable crystal modification (form I with a hexagonal unit cell) with a melting point of 134°C from d.s.c. measurements and from WAXD studies. The weight-average crystallinity is 60% from the WAXD measurement (the detailed procedures will be presented elsewhere[19]) and 65% from the d.s.c. measurements, assuming the true heat of fusion of the crystal to be 30 cal/g.

Figure 1 shows a typical electron micrograph of surface replicas of the specimens. The centres of the sheaf-like crystalline superstructures are oriented along the extrusion direction (ED). Stacks of lamellae are highly oriented with their nomals (i.e. chain direction) parallel to the ED. These lamellae are supposed to overgrow from 'rows' of nucleating points (oriented nearly parallel to the ED), initially, in a direction normal to the ED. In the course of its overgrowth, however, the growing front may occasionally branch at some distances and angles in space into new lamellae, resulting in the development of the diverging sheaf of lamellae as shown in the micrograph. We will designate the superstructure as 'row-nucleated' sheaf-like superstructure for the sake of convenience. The radius and aperture angle of the sheaves were found to depend upon crystallization conditions. For an example both the radius and aperture angle decrease with increasing molecular orientation in melts. For the film specimens studied in this article, the radius and aperture angle were 3 μm and 30°, respectively, from the micrograph and the SALS studies as will be described later. The surface structure observed in the electron micrograph has been confirmed to represent properly the internal structure of the materials with SALS studies and SAXS patterns as will be discussed later.

A marked mechanical anisotropy was observed; the initial Young's moduli are 3.6, 2.8 and 4.7 kg/cm^2 along the ED, at 45°-direction to it, and in the transverse direction (TD), respectively, and the elongations at break are 130, 290 and 390% in the respective directions. When the specimens are stretched along the ED, they uniformly begin to whiten at 5% elongation. The whitening of the specimens when stretched along other directions than the ED is not as marked as that observed upon stretching along the ED.

When the specimens are stretched along the ED at temperatures above the glass transition temperature of polybutene-1, they exhibit a remarkably large length-recovery from large extensions as shown in *Figure 2* where the stress-strain behaviour under cyclic loading is shown as a function of temperature. Near or below the glass transition temperatures, the specimens break at each elongation percent as shown in the figure and do not exhibit the unique long-range elasticity observed at higher temperatures.

Figure 3 shows the corresponding stress-strain behaviour of polybutene-1 films crystallized from isotropic melts and subsequently annealed at 100°C for about 5 h to assure the crystal being a stable modification as in the blown films. It is apparent that the isotropic films do not exhibit the long-range elasticity as the blown films do. Thus the long-range elasticity strongly depends upon morphology of the superstructure. Consequently the morphology of the superstructure and its deformation behaviour will be studied in detail in following sections. We will discuss also the long-

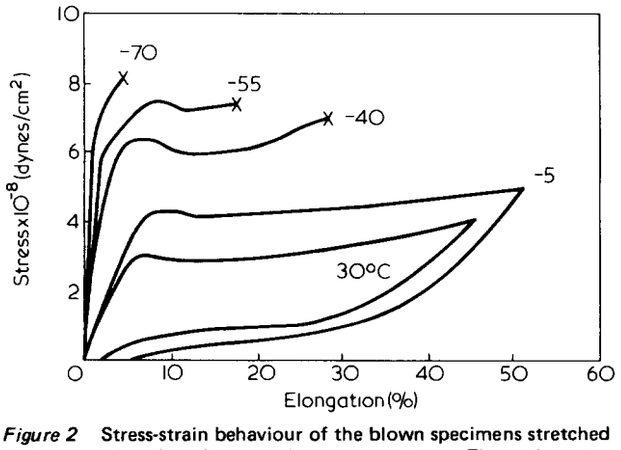

Figure 2 Stress-strain behaviour of the blown specimens stretched in the extrusion direction at various temperatures. Elongation rate, 100%/min

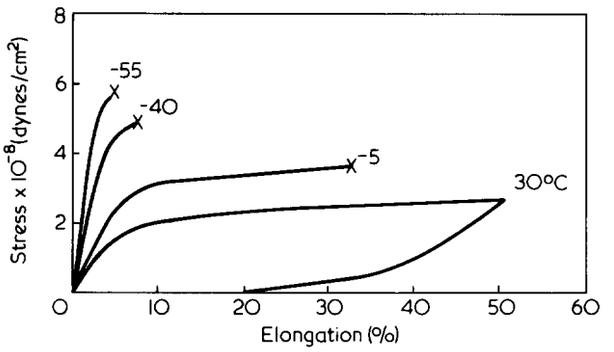

Figure 3 Stress-strain behaviour of the polybutene-1 films crystallized from an isotropic melt. Elongation rate, 100%/min

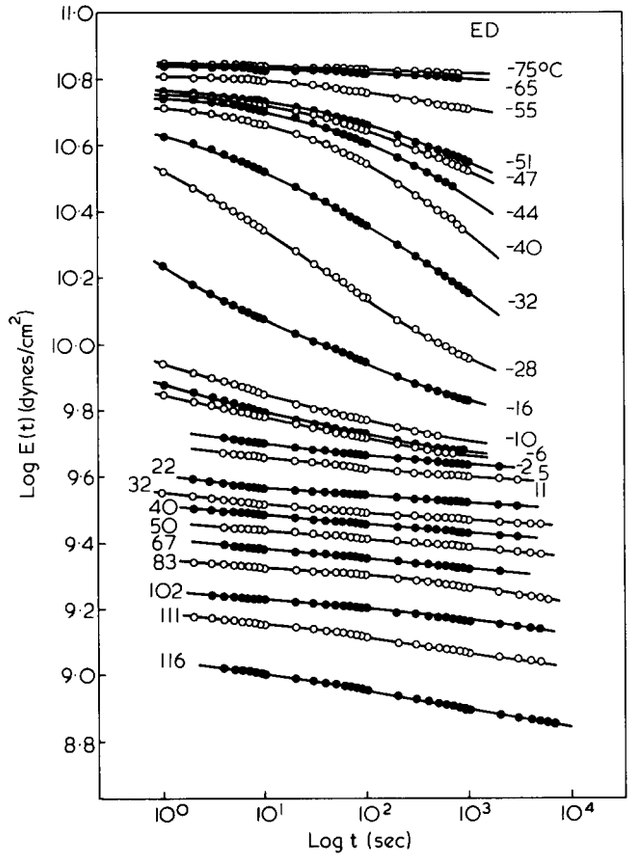

Figure 4 Stress relaxation behaviour of the specimens along the ED at various temperatures

range elasticity of the films in comparison with the long-range elasticity as reported for other 'hard-elastic' or 'springy' materials.

Since the mechanical properties and probably the deformation behaviour also depend on mobility of molecular motion, it would be worthwhile to present mechanical relaxation behaviour in the linear viscoelastic region. *Figure 4* represents the stress relaxation moduli as a function of time and temperature, and *Figure 5* represents the isochronal relaxation modulus at 100 sec as a function of temperature, the strain being applied parallel to the extrusion direction in both cases. A large stress relaxation apparently occurs at $-50°$ to 0°C which may be attributed to molecular motion in the amorphous phase. It should be noted, however, that some of the molecular motion in the amorphous phase should occur in cooperation with the deformation of lamellar crystals, owing to the special morphology as described in following sections. The effect of such cooperation on the viscoelastic properties will be discussed elsewhere[19].

The isothermal stress relaxations at higher temperatures (i.e. 0 ~ 100°C) are surprisingly small as shown in *Figure 4*, and the decrease of the isochronal relaxation modulus in the temperature range may be described in terms of decreased modulus of crystals plus a minor contribution from relaxation associated with the amorphous phase[19].

EXPERIMENTAL

Wide-angle X-ray diffraction (WAXD) patterns and small-angle X-ray scattering (SAXS) patterns were obtained, respectively, at 40 kV, 20 mA, and 40 kV, 100 mA (using a Rotaflex RU-100PL, Rigaku-denki) with nickel-filtered CuKα radiation. The SAXS patterns were taken with a point focussing system under the following collimation conditions: distances of the second pinhole, specimen, and photographic films were 250, 310, and 610 mm from the first pinhole, respectively, and the size of the first and second pinholes were 0.5 and 0.2 mm in diameter, respectively.

Both SAXS and WAXD patterns were recorded from three directions in order to study the symmetry of orientation distribution of crystallites and lamellar platelets: 'end' patterns taken with the incident X-ray beam parallel to the extrusion direction (ED), 'through' patterns with the beam normal to the ED and to the film surface, and 'edge' patterns with the beam normal to the ED but parallel to the film surface.

For the undeformed films and those stretched along the ED, the end patterns are circular symmetric, and the edge and through patterns are equivalent, indicating that the orientation of the crystallites and the lamellar platelets are *uniaxially symmetric* with ED.

The SAXS intensity distributions were measured along the meridional direction, i.e. a direction parallel to ED with line focussing under the following collimating system: the second slit, the specimen, and the third and fourth slits which were placed, respectively, in front of and after the Soller slits were placed at 250, 310, 570, and 610 mm from the first

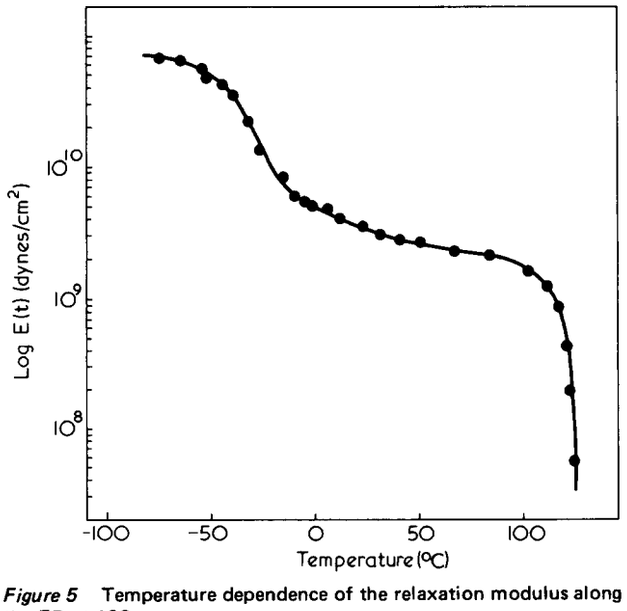

Figure 5 Temperature dependence of the relaxation modulus along the ED at 100 sec

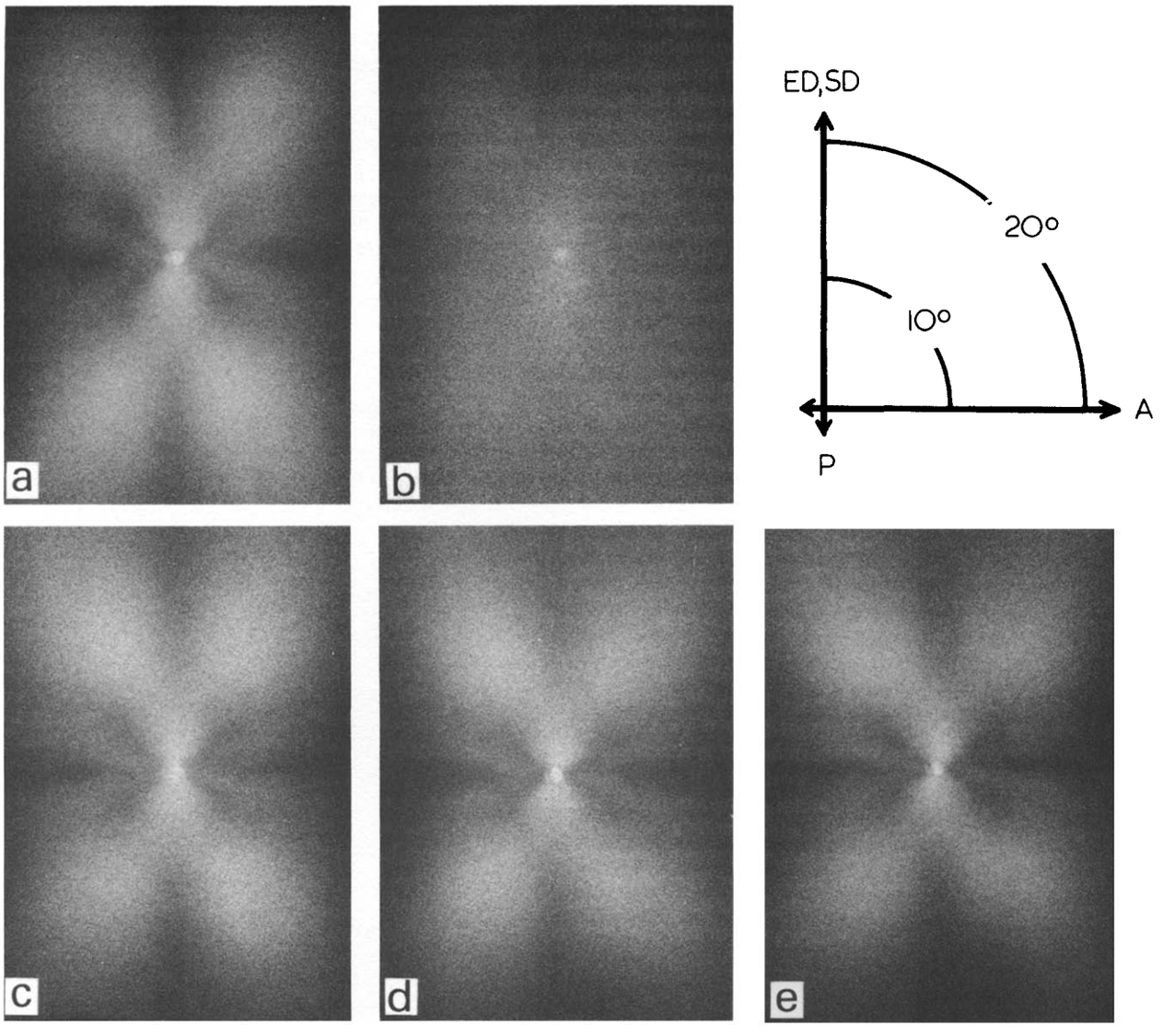

Figure 6 Depolarized light scattering patterns for (a) undeformed specimen, (b) specimens stretched by 5% elongation. The patterns shown in (c) to (e) are taken for specimens stretched by 5%, 15%, 30%, respectively, and then immersed in silicone oil of refractive index of 1.56. The symbols SD, P and A stand for stretching direction, polarization direction of polarizer and analyser, respectively

slit, respectively, and the sizes of the first, second, third and fourth slits were 0.1 x 10, 0.1 x 10, 0.1 x 15, and 0.05 x 15 mm^2, respectively. The length direction of the slits and focal spot were set normal to the ED, i.e., parallel to the stack of lamellae, to minimize the slit blurring effect[20] of scattered X-rays. The intensity was measured with a scintillation counter and pulse height analyser and with nickel filtered CuKα radiation operated at 40 kV, 100 mA.

The second-order orientation factor of crystal *c*-axis of the stable crystal modification was evaluated by measuring the azimuthal angle dependence of integrated intensities under diffraction peaks corresponding to the (110) and (300) crystal planes. The orientation factor obtained from the two crystal planes was identical within experimental accuracy.

DEFORMATION BEHAVIOUR

Sheaf-like crystalline superstructure

The deformation mechanism of the sheaf-like crystalline superstructure was studied by SALS experiments. *Figure 6* represents typical change of depolarized light scattering patterns upon stretching along the ED. When the specimens are stretched along the ED, they become increasingly opaque so that the scattering patterns are significantly distorted by multiple scattering as shown in *Figure 6b*. In order to study the scattering from the internal superstructure, the difficulty arising from the multiple scattering was avoided in *Figures 6c* to *6e* by immersing the stretched specimens between microscope cover glasses in a silicone oil having similar refractive index to the specimens. Without affecting morphology, the oil interpenetrates the interlamellar voids, reduces the scattering from voids, and thus minimizes the multiple scattering effect.

As seen in *Figure 6*, upon stretching along the ED, the original 'butterfly' type pattern which is oriented along the meridian due to orientation of the sheaf with its radii along the TD tends to become more circularly symmetric, indicating that the superstructure tends to become more spherically symmetric. A possible deformation mechanism is represented schematically in *Figure 7* where it is shown that the stretching involves an increase of the aperture angle from γ_0 to γ_λ.

The analyses of the depolarized light scattering patterns in

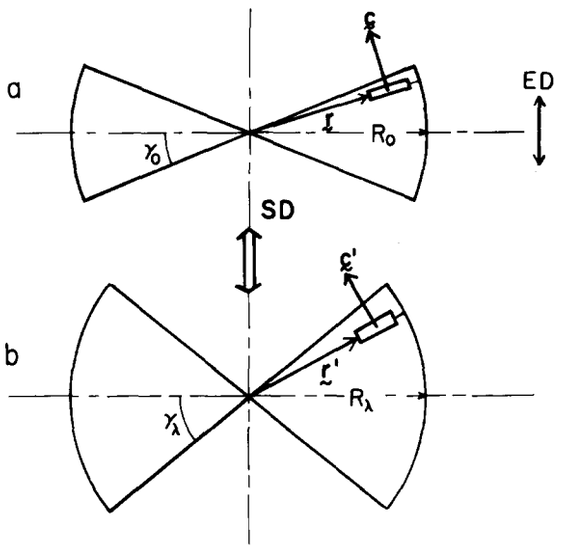

Figure 7 Schematic diagram showing deformation behaviour of the sheaf-like crystalline superstructure, (a) undeformed and (b) deformed states. The stretching direction (SD) and extrusion direction (ED) are both vertical

terms of the scattering angle θ_{max} and azimuthal angle μ_{max} of maximum intensity have been shown to yield information on the deformation of the sheaf-like superstructure with R_λ and γ_λ. The detailed procedure in evaluating the parameters has been described elsewhere[21,22]. *Figure 8* represents a change of the aperture angle γ_λ of the sheaf relative to the original angle γ_0 with applied elongation (open circles). The solid line corresponds to the calculated γ_λ/γ_0 based upon affine deformation of the sheaf with increasing volume under the condition $\lambda_1 = \lambda_2 = 0.7 + 0.3\,\lambda_3^{-1}$ and $\lambda_3 = \lambda_B$ where $\lambda_1 = \lambda_2$, and λ_3 are the extension ratios of the sheaf along the TD and ED, respectively. A fine agreement between the calculated and observed results indicates that the affine deformation is a good approximation in describing the deformation of the sheaf. However, the radius of the sheaf R_λ hardly changes with the deformation and $R_\lambda/R_0 \simeq 1$, the plot of which was not therefore included in the figure. This mode of deformation of the sheaves is capable of accounting for volume dilatation of bulk specimens, and in the next section we will discuss how the volume increase of the sheaves is incorporated with deformation of the submicroscopic structural units.

The solid circles indicate the residual values of γ_λ/γ_0 for the specimens completely released from each elongation percent. This result will be discussed later in connection with recoverability of deformation.

Lamellar network

In this section we shall discuss deformation of lamellae constituting the sheaf-like microscopic structure as observed by the small-angle X-ray scattering technique.

Figure 9 represents change of SAXS patterns upon stretching the specimens along the ED. The SAXS patterns for the undeformed and deformed specimen are typical of two-point patterns with their lateral breadths increasing with increasing stretching. The increase of the breadth may be primarily attributed to an increase of the aperture angle of the sheaf as analysed from SALS patterns (see *Figure 8*). One of the striking effects of stretching is a tremendous increase of scattered intensity. The intensity increases two orders of magnitude upon stretching 50% along the ED. The paterns taken with shorter exposure times also clearly show a decreased scattering angle $2\theta_{max}$ of the maximum intensity and therefore an increase of the long identity period of the lamellar system.

The tremendous increase of the SAXS intensity and systematic decrease of $2\theta_{max}$ are more quantitatively represented in *Figure 10* in which the meridional SAXS intensity distributions are plotted for undeformed and deformed specimens. It is important to note that the relative intensity distributions are essentially unchanged with elongations, and only absolute intensity is changed. This indicates that the deformation does not involve large heterogeneous deformation but rather uniform deformation of the lamellar network, involving bending type deformation of lamellae, splaying apart of the interlamellar spacings and generating the interlamellar voids or density lowering. Thus the deformation increases the mean-square electron density fluctuations.

This is further confirmed by a result shown in *Figure 11* in which the meridional SAXS intensity distributions were measured by immersing the stretched specimens in liquid paraffin (SG 0.855). The liquid paraffin penetrates interlamellar regions, increases the electron density of the interlamellar amorphous layer to a value approximately equal to that of the amorphous layer in the undeformed state, and thus decreases the SAXS intensity to a level nearly equivalent to the intensity for the undeformed specimens. The interlamellar spacings are clearly seen to be increased systematically upon stretching. The relative intensity distributions are seen to be essentially unaltered, indicating that the paracrystalline order of the interlamellar spacings tends to be maintained up to the high elongations. This again indicates a very uniform deformation of the lamellar assembly.

The interlamellar spacing L was evaluated by applying Bragg's law for the scattering angle $2\theta_{max}$ of the first intensity maximum in the meridional intensity distribution of the stretched and immersed specimens;

$$2L \sin\theta_{max} = \lambda \qquad (1)$$

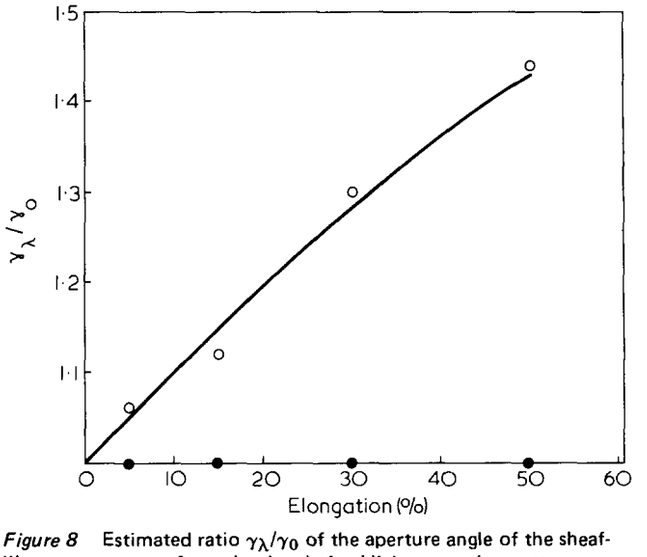

Figure 8 Estimated ratio γ_λ/γ_0 of the aperture angle of the sheaf-like superstructure from the depolarized light scattering patterns (open circles). The solid line corresponds to the calculated γ_λ/γ_0 based on affine deformation with increasing volume ($\lambda_1 = \lambda_2 = 0.7 + 0.3\lambda_3^{-1}$, $\lambda_3 = \lambda_B$, $\lambda_1 = \lambda_2$ and λ_3 being extrusion ratios along the TD and ED, respectively). The solid circles represent residual deformation of the aperture angle (γ_λ/γ_0) upon releasing the bulk specimen from a given applied elongation. λ_B is the extension ratio of the bulk specimen

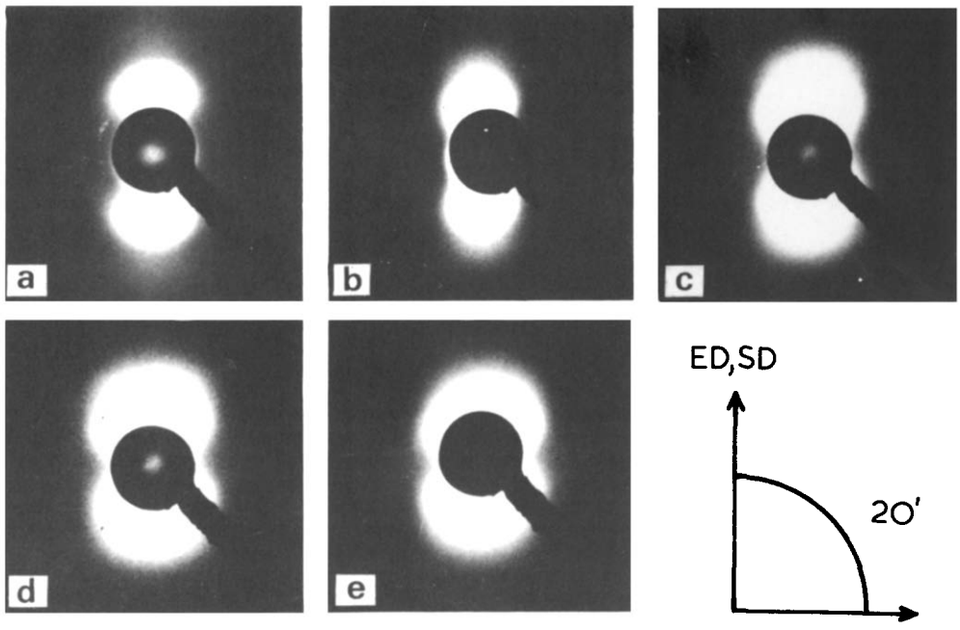

Figure 9 Variation of SAXS patterns with stretching along the ED (vertical direction of the figure). (a) 0%, (b) 15%, (c) 30%, (d) 50%, and (e) 80%

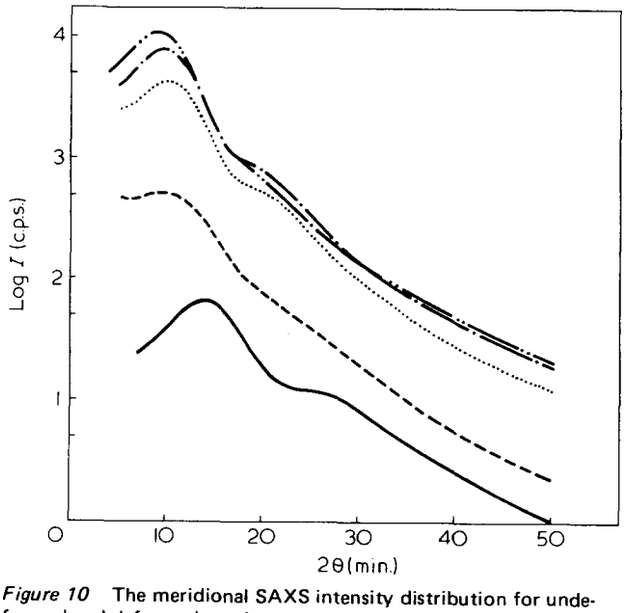

Figure 10 The meridional SAXS intensity distribution for undeformed and deformed specimens. ——— unstretched; — — — — 5% stretched; . . . . . 15% stretched; — · — · — 30% stretched; — · · — stretched

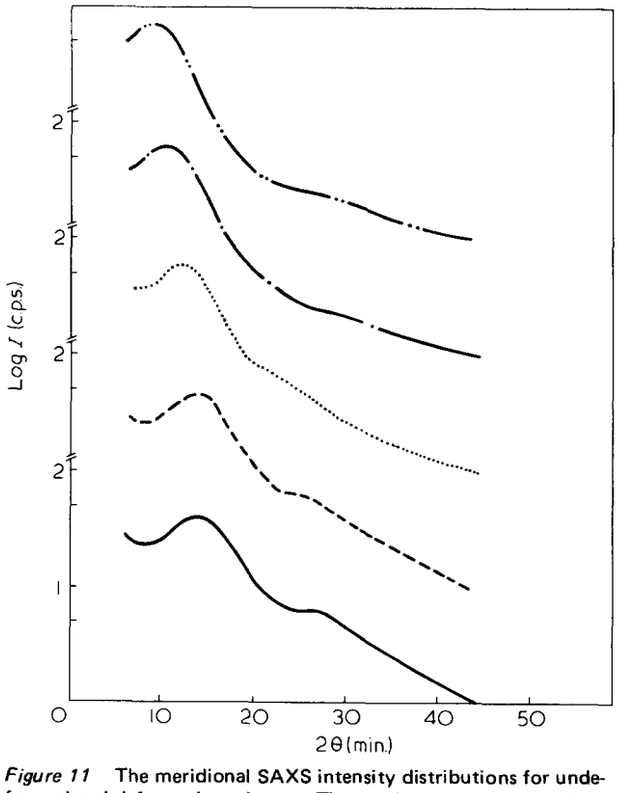

Figure 11 The meridional SAXS intensity distributions for undeformed and deformed specimens. The specimens are immersed in a liquid paraffin in the deformed state. Key as *Figure 10*

Figure 12 shows the deformation (in percentage elongation) of the interlamellar spacing $\Delta L/L_0 = (L - L_0)/L_0$ (L_0 being the spacing for the undeformed specimen) in relation to the bulk elongation of the specimens. It is clearly observed that the bulk strain is essentially identical to the submicroscopic strain, i.e. the strain in the interlamellar spacings. The figure also indicates the residual strain (in percentage elongation, solid circles) in interlamellar spacings for the specimens stretched at a given percentage elongation and then relaxed as a function of percentage elongation. The recovery of the spacing will be discussed later.

The equality of the submicroscopic strain and the bulk strain, and the homogeneities of the submicroscopic deformation are believed to be the most important phenomena in understanding the deformation behaviour and mechanical properties of the blown films. This leads to the local submicroscopic deformation being added to the bulk deformation, and the stress effective to the deformation is homogeneous. In order to confirm this conclusion and to obtain some insight into the deformation of the interlamellar amorphous phase, we have analysed the relative change of the SAXS intensity with elongation immediately below.

The change of SAXS intensity may be interpreted in terms

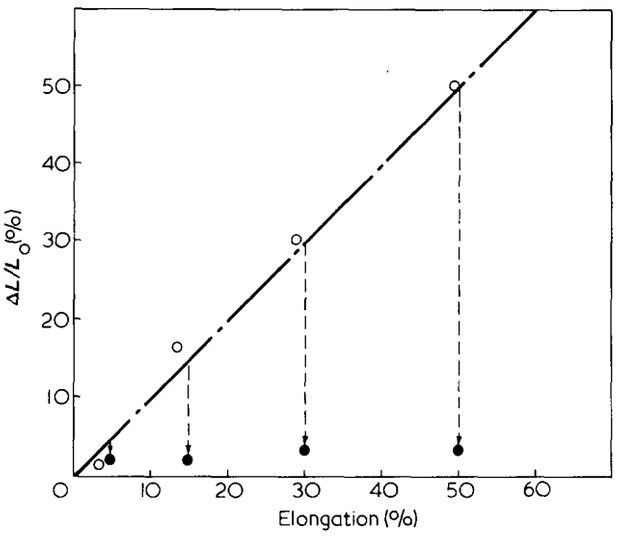

Figure 12 Percentage elongation of interlamellar spacing $\Delta L/L_0$ as a function of bulk elongation (open circles) and residual elongation of the spacing upon releasing the bulk specimens from each bulk elongation (solid circles)

of a one-dimensional paracrystalline assembly of lamellae, i.e. the stack of lamellae parallel to one another with their chain axes parallel to the ED. As will be discussed in detail in the Appendix, the scattering intensity of the nth order maximum corrected for the diffuse background scattering $I_L(b_n)$ is given by

$$I_L(b_n) \sim n^{-4}N(L/g)^2(\rho_c - \rho_a)^2\sin^2(\pi n\phi_c) \qquad (2)$$

where N is the number of lamellae in the assembly, L and ϕ_c are the average long spacing of the lamellae and volume average crystallinity, respectively. ρ_c and ρ_a are the electron densities of lamellae and interlamellar region, respectively, and g is the paracrystalline disorder parameter defined by

$$g = \Delta/L \qquad (3)$$

where Δ is the fluctuation of the lamellar spacing from the mean value L. Thus the change of the nth order scattering maximum with elongation is described in terms of the change of the quantity N, g or Δ, L, $(\rho_c - \rho_a)^2$, and ϕ_c.

We assume that the density ρ_c does not vary with elongation, equal to $\rho_{c,0}$ in the undeformed state, while the density ρ_a is *uniformly lowered* from $\rho_{a,0}$ in the undeformed state owing to the splaying apart of the interlamellar spacing:

$$\rho_c = \rho_{c,0}$$

$$\rho_a = \rho_{a,0}(l_0/l) = \rho_{a,0}\frac{1 - a/L_0}{L/L_0 - a/L_0} = \rho_{a,0}\frac{1 - \phi_{c,0}}{\lambda - \phi_{c,0}} \qquad (4)$$

where l_0 and l are the thickness of the amorphous layer in the undeformed and deformed state, a is the thickness of the lamellae, and $\phi_{c,0}$ is the volume-average crystallinity in the undeformed state. $\phi_{c,0}$ is related to ϕ_c by

$$\phi_c = \phi_{c,0}(L_0/L) = \phi_{c,0}/\lambda \qquad (5)$$

λ is the extension ratio of the interlamellar spacing.

Figure 13 represents the relative change of the $I_L(b_1)$, i.e. the intensity of the first order scattering maximum corrected for the background scattering (open circles) and that of the $I_L(b_1)$ calculated from equations (2)–(5). In order to obtain the relative intensity, $I_L(b_1)$ at a given elongation was divided by $I_L^0(b_1)$ for undeformed specimens. The calculated results were obtained for $\rho_{c,0} = 0.951$ and $\rho_{a,0} = 0.870$ g/cm^3, $\phi_{c,0} = 0.6$ (measured from X-ray diffraction and differential scanning calorimetry). The quantity $\lambda = L/L_0$ was estimated from SAXS measurements (*Figure 12*). The quantity N was assumed to be invariant with stretching, which may be legitimate in the light of experimentally assured uniform deformation of the lamellar assembly. The calculated curves A and B were obtained, respectively, for the cases where Δ and $g = \Delta/L$ are invariant with the stretching. Thus it was confirmed that the measured relative intensity can be described in terms of the one-dimensional paracrystal model and the uniform density lowering in the interlamellar amorphous layer as a consequence of splaying apart of the interlamellar spacing. The curve (A) fits better with the experimental results, which again reflects the uniform deformation of the lamellar assembly.

It should be noted that the measured intensity ratios (open circles) tend to be levelled off at high elongation. This is due to the disorientation of the lamellar assembly (corresponding to the decrease of the second order orientation factor f_c with elongations as discussed in next section) with respect to the stretching direction. The effect of the disorientation was corrected for by multiplying the ratio of the orientation factors $f_c(\lambda)/f_c(\lambda = 1)$ (λ being the extension ratio) by the measured intensity ratio $I_L(b_1)/I_L^0(b_1)$ to facilitate the comparison with the theoretical ratio evaluated for the perfectly oriented system. The corrected intensity ratios are represented by solid circles in *Figure 13*. It turns out that the correction gives a better agreement with the calculated curve (A).

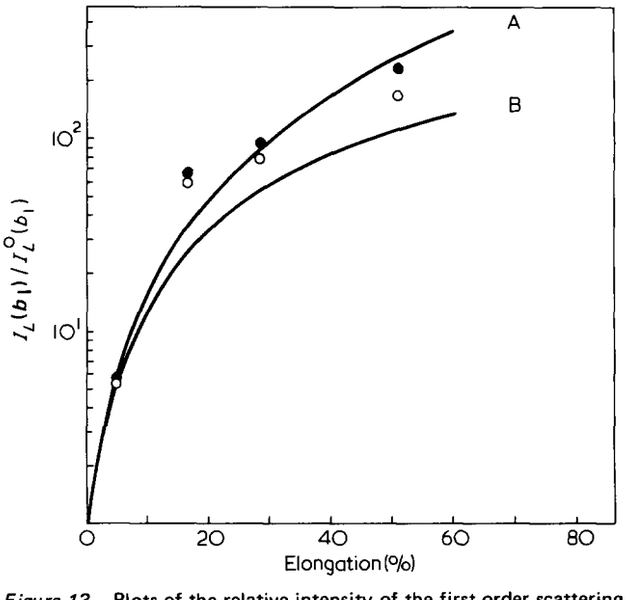

Figure 13 Plots of the relative intensity of the first order scattering maximum $I_L(b_1)/I_L^0(b_1)$ as a function of percentage elongation. The open and solid circles correspond to the measured ratios $I_L(b_1)/I_L^0(b_1)$ which are uncorrected and corrected for the disorientation of the lamellar assembly, respectively. The curves A and B correspond to the calculated ratios for the cases where Δ and g are invariant with the percentage elongation respectively. $I_L^0(b_1)$ is the intensity of the first-order scattering maximum for undeformed specimen. The calculated ratios are obtained for $\rho_{c,0} = 0.951$, $\rho_{a,0} = 0.870$ g/cm^3, and $\phi_{c,0} = 0.6$

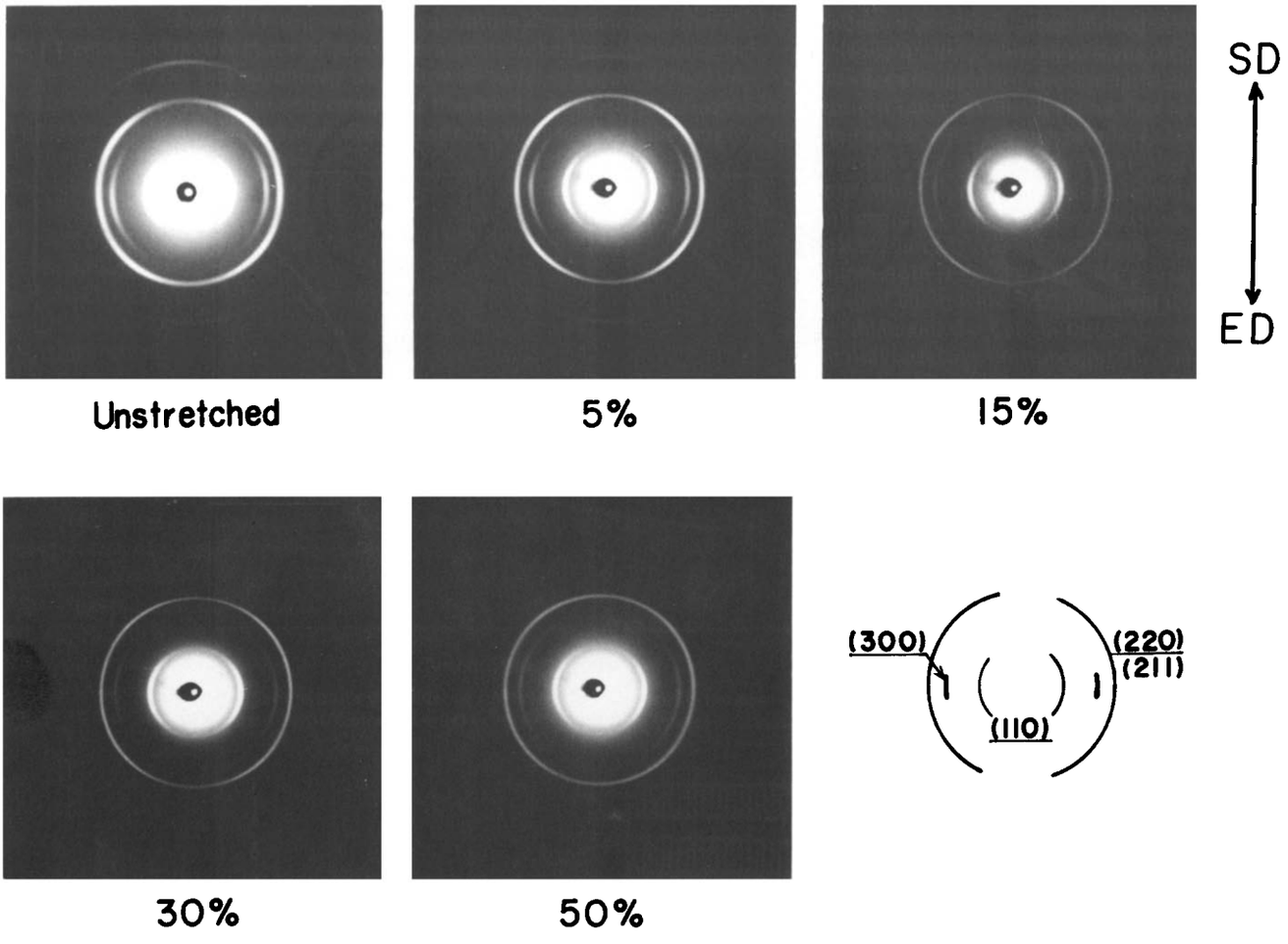

Figure 14 Variation of the WAXD patterns with stretching along the ED. The stretching direction (SD) and ED are vertical

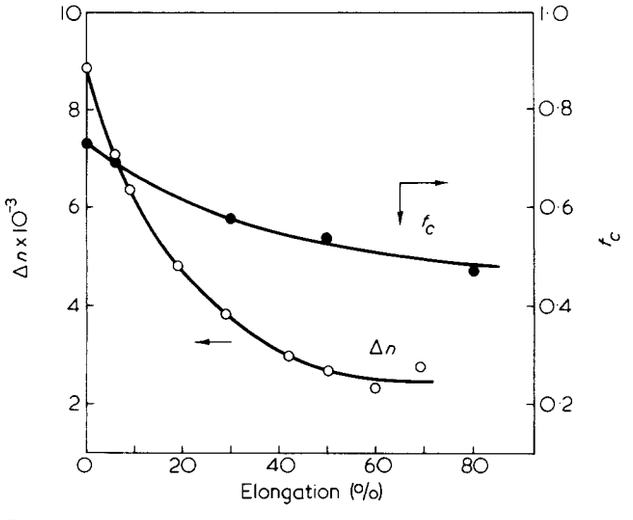

Figure 15 Change of the second-order orientation factor $f_c = [3\langle\cos^2\theta_c\rangle - 1]/2$ and the birefringence Δn with stretching. Δn was measured by immersing the stretched specimens in ethyl alcohol

Therefore the SAXS studies can add further information to the deformation behaviour of the sheaf-like crystalline superstructure as obtained by SALS studies (*Figure 7*); accompanied by the affine deformation of the sheaf-like superstructure, the lamellae tend to disorient as indicated by orientation of a lamellar axis from $\underset{\sim}{r}$ to $\underset{\sim}{r}'$ (*Figure 7*) and bend between tie links, resulting in the expansion of the interlamellar spacing and density-lowering of the interlamellar amorphous layer. There is also one to one correspondence of the deformation of the submicroscopic structural unit and the bulk specimen.

Molecular orientation

In the preceding sections, the deformation behaviour of the bulk specimen was studied in terms of the microscopic and submicroscopic structures. In this section we will study it in terms of molecular orientation in crystalline and amorphous regions.

Figure 14 represents the WAXD patterns upon stretching along the ED. It is obvious from the figure that the diffraction from the planes (*hk0*) parallel to the crystal *c*-axis becomes less dependent upon the azimuthal angle with stretching, indicating that the crystal *c*-axis tends to disorient with stretching. The disorientation is more quantitatively demonstrated in *Figure 15* where the second-order orientation factor

$$f_c = [3\langle\cos^2\theta_c\rangle - 1]/2$$

θ_c being an angle between the stretching direction and the *c*-axis, as well as birefringence Δn are shown as a function of percentage elongation. The f_c decreases from about 0.73 to 0.47 with stretching the undeformed films by 80%.

The decrease of f_c is interpreted in terms of orientation of the lamellar axis (from $\underset{\sim}{r}$ to $\underset{\sim}{r}'$ in *Figure 7*) toward the stretching direction accompanied by the deformation of the

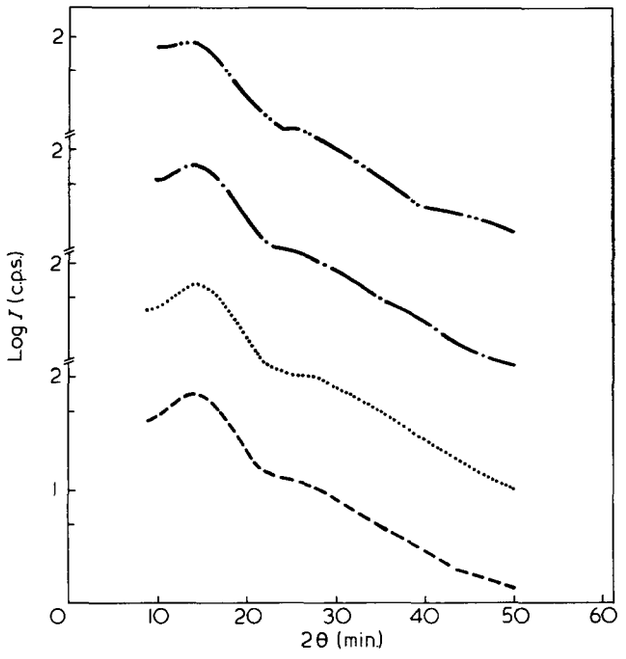

Figure 16 The meridional SAXS intensity distributions for the specimens released from each bulk elongation percent. Key as *Figure 10*

sheaf. Since the *c*-axis orients nearly tangentially to the radius of the sheaf, the increase of the aperture angle decreases the value of f_c. At this point one should note the role of lamellar twisting on the crystal orientation behaviour; i.e., upon stretching, the twisted lamellae tend to be untwisted around their axes in such a manner that the chain axes orient along the stretching direction. The untwisting mechanism thus gives rise to an increase in the crystal *c*-axis orientation and is probably an important mechanism which accounts for a positive *c*-axis orientation in spherulitic films[1–5,10] and in the oriented-crystallized films of polyethylene having row-nucleated cylindritic morphology[12,23]. If this mechanism occurs in the polybutene-1 films, it should tend to compensate the negative *c*-axis orientation mechanism. The fact that the f_c monotonically decreases with stretching indicates that the contribution of the untwisting mechanism to the f_c is only minor, suggesting that the lamellae are not twisted extensively and/or reluctant to be untwisted.

The amorphous chain orientation may be estimated by the birefringence measurement and by separating the contribution of the amorphous chain orientation (Δ_{am}) from the total birefringence Δn. Since the specimen whitens uniformly upon stretching, Δn cannot be measured without immersing the specimens at elongations greater than 10% in a liquid to reduce the opaqueness. Δn in the figure was measured by immersing the stretched specimens in ethyl alcohol. Detailed analyses of the birefringence (which will be described in detail in a later paper[18]) have shown that even in the immersed specimen, Δ_{form} is significant and comparable with the birefringence arising from the crystal orientation Δ_{cr} and the amorphous chain orientation Δ_{am}. It turns out that the decrease of Δn is primarily attributed to the decrease of Δ_{form} (or increase of Δ_{form}) and of the Δ_{cr}. The decrease of Δ_{form} is due to the interlamellar density-lowering which results in the negative form birefringence, while the decrease of Δ_{cr} is due to the decrease of f_c. Thus the studies of the molecular orientation also confirm the proposed deformation mechanism described in previous sections in terms of the SALS and SAXS studies.

RECOVERABILITY OF DEFORMATION

In order to understand a unique mechanical property of the films at temperatures above the glass transition, i.e., a high degree of length recovery from large extensions, we have studied the recoverability of deformation upon releasing applied strain in terms of bulk dimensions, the microscopic and submicroscopic structural elements and molecular orientation in crystalline and amorphous regions.

Bulk

The length recovery of bulk specimens above the glass transition temperatures was almost perfect. The residual elongation was only a few percent even for the specimens stretched by about 80%.

Microscopic structure

Recoverability of deformation of the sheaf-like superstructure was studied as a function of the initial percentage elongation of the bulk specimens. The results on the recoverability of the aperture angle γ_λ/γ_0 is included in *Figure 8* (solid circles). The result shows a complete recovery of the sheaf deformation, which in turn is a structural origin of the length recovery of bulk specimens.

Submicroscopic structure

Recoverability of deformation of the lamellar network, i.e., a stack of oriented lamellae which are linked by tie links (amorphous and/or crystalline links), was studied with the SAXS intensity distribution for the specimens released from various amounts of extensions. As represented in *Figure 16* the SAXS intensity distributions for the relaxed specimens become almost identical to that for the undeformed specimen. *Figure 12* which includes residual elongation of the interlamellar spacing $\Delta L/L_0$ as a function of bulk elongations (solid circles) shows that the submicroscopic deformation is also recoverable to within a small residual percentage elongation. This is also associated with the length recovery of bulk specimens from large extension. The SAXS intensity distribution for the specimens relaxed from 50% elongation shows a little smoothed distribution compared with those from the specimens relaxed from lower elongations. This may be due to an imperfect recovery (although not significant) of the disorders of the lamellar network involved in the bulk deformation. The intensity level and the peak positions, however, are almost completely recovered.

Thus the evidence obtained on the deformation and recoverability of the structure in the microscopic and submicroscopic levels leads to the conclusion that the row-nucleated sheaf-like superstructure is deformed affinely to the bulk deformation, the aperture angles of the sheaves being affinely increased but their radii being kept almost constant. This deformation which leads to a volume dilatation, and an apparent decrease of density of bulk specimens occurs in conjunction with orientation and uniform deformation of the internal structural units, i.e., the lamella axes being oriented toward the stretching direction and the interlamellar spacing being expanded by the mechanism which involves the lamellar bending between tie links (referring to crystal bridge as envisaged by Clark[13,14]) and/or tie chains.

Since the deformation of the interlamellar spacing is uni-

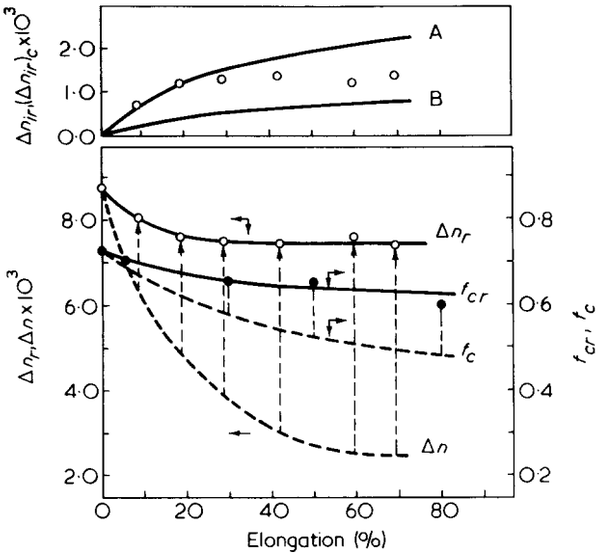

Figure 17 Plots of residual second-order orientation factor ($f_{c,r}$) and residual total birefringence (Δn_r) as a function of bulk elongations, f_c and Δn measured in stretching cycles were also included as a reference. Plots of unrecoverable amount of total birefringence Δn_{ir} (= $\Delta n_0 - \Delta n_r$, Δn_0 being birefringence of undeformed dry specimen) (open circles) and that of birefringence arising from unrecoverable crystal orientation $(\Delta n_{ir})_c$ (= $(f_{c,0} - f_{c,r})\phi_{c,r}\Delta_c^0$, $f_{c,0}$ being the orientation factor of the undeformed specimen, $\phi_{c,r}$ being the volume-average crystallinity of each relaxed specimen) for Δ_c^0 = 0.034 (curve A) and 0.0108 (curve B)

form and cumulative, a small increase of the interlamellar spacing resulting from deformation of lamellae (bending of the lamellae between tie links in a manner analogous to a leaf spring) and of tie links (or tie chains) within their elastic limits accounts for the large recoverable deformation of the bulk specimens and the recoverable deformation of the sheaves. The sheaves impinge onto each other and the intersheaf region between the two impinged sheaves should be mechanically strong and should not yield. The origin of the elastic restoring force is discussed in detail in the following section in connection with the springy properties. First the recoverability of the molecular orientation is discussed

Molecular orientation

Recoverability of molecular orientation upon releasing the applied strain was investigated in terms of the recoverability of Δn and f_c. *Figure 17* represents the residual second-order orientation factor of the crystal c-axis, $f_{c,r}$, and residual total birefringence Δn_r. The figure includes the values of f_c and Δn shown in *Figure 15* (broken lines) for reference. A remarkable amount of irreversible molecular orientation exists, as manifested in Δn_r and $f_{c,r}$ despite the fact that the submicroscopic and microscopic deformations are all recoverable.

The figure also includes the unrecoverable amount of total birefringence $\Delta n_{ir} = \Delta n_0 - \Delta n_r$ (open circles) where Δn_0 is birefringence of the undeformed dry specimen and birefringence arising from unreocverable crystal orientation, $(\Delta n_{ir})_c = (f_{c,0} - f_{c,r})\phi_{c,r}\Delta_c^0$ (solid line) where $f_{c,0}$ is the orientation factor of the undeformed specimen, $\phi_{c,r}$ is the volume-average crystallinity of each relaxed specimen (which should be identical to $\phi_{c,0}$) and Δ_c^0 is the intrinsic birefringence of the stable crystal modification (0.034[24] or 0.0108[25]). Although the absolute value of $(\Delta n_{ir})_c$ involves some uncertainty due to the uncertainty of Δ_c^0, the result indicates that the unrecoverable amount of total birefringence arises both from the irreversible crystal orientation and amorphous chain orientation. However, the irreversible crystal and amorphous orientations are found not to contribute residual bulk strain. This is because the local strain effective to the orientations may be only a minor fraction of bulk strain (the displacement of the interlamellar spacing being a major contribution to the bulk strain). The discussions on the detailed mechanism leading to the unrecoverable molecular orientations are beyond the scope of this article, but this may be apparently related to the work softening properties of the specimens as depicted in *Figure 18* which shows the stress–strain property under cyclic tensile loading along the ED at room temperature.

SPRINGY PROPERTIES OF THE BLOWN FILMS

It would be worthwhile to compare the apparent springy properties of the polybutene-1 films with those of other polymers such as Celcon fibres[13–17]. From the discussions in the preceding sections, it is obvious that the special properties observed at temperatures above the glass transition such as a high degree of length recovery from large extensions, a marked reduction of apparent density and increased turbidity of the films are essentially the same as those observed for other springy materials[13–17]. As in other materials, these special properties are shown to be attributed to the special morphology of the polybutene-1 films, i.e., the stacks of oriented lamellae, which itself is essentially identical to other materials. Owing to the special morphology, the deformations of the interlamellar spacings are uniform and the small deformations within their elastic limits are additive in the lamellar aggregate to produce a large recoverable deformation of the bulk specimens. It is central to the springy properties to understand whether these elastic deformations originate from the elastic lamellar bending between the tie links in a manner analogous to a leaf spring[13,14] or from the elasticity of the amorphous tie chains which is essentially entropic.

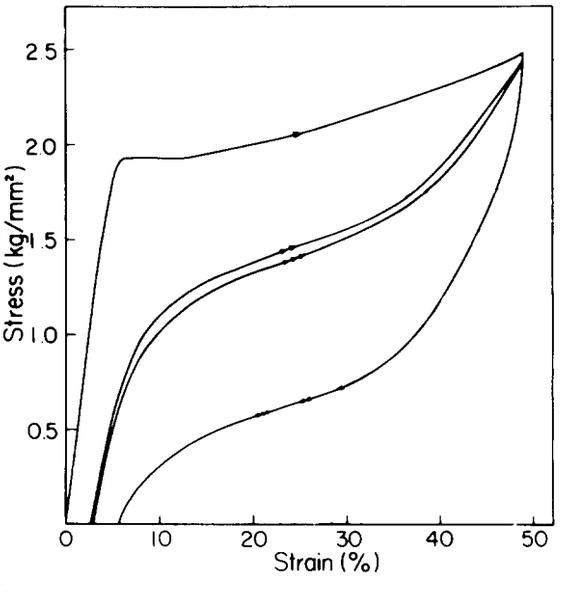

Figure 18 Stress-strain behaviour under cyclic tensile loading of the polybutene-1 films along the ED. Number of arrows indicates the cycle number

Figure 19 respresents temperature dependence of the retractive force of the specimens stretched by 30% along the ED. The specimens were allowed to relax about 300 sec before the measurements of the force. As in other springy materials the retractive force drops with temperature, suggesting an apparent energy driven elasticity[15–17].

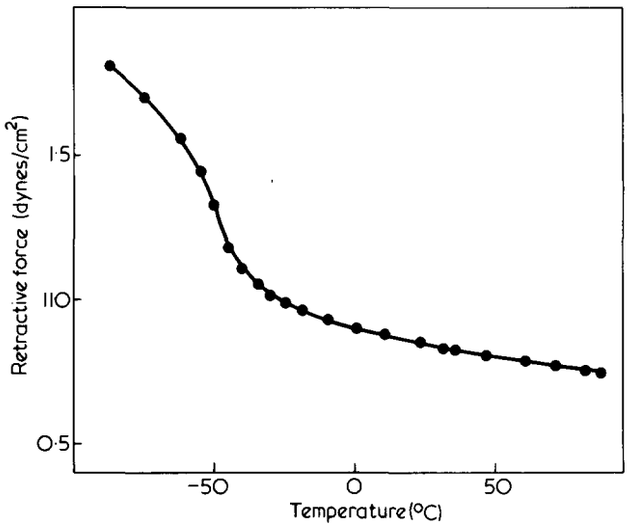

Figure 19 Temperature dependence of the retractive force of the specimens stretched by 30% along the ED

However there exist significant differences between this result and that obtained for the springy Celcon fibres[15–17]: (1) the retractive force is smaller than that of the Celcon fibre by one to two orders of magnitude, (2) the temperature coefficient is ca. -2×10^4 dynes/cm^2 deg for the polybutene-1 films, while that of the Celcon fibre is ca. -1.6×10^6 dynes/cm^2 deg, thus the coefficient is two orders of magnitude smaller, and (3) change of the coefficient at glass transition temperature is more drastic for the polybutene-1 films than for the Celcon fibre. A fundamental difference between this specimen and the Celcon fibres also exists in the point that the polybutene-1 films exhibit the long-range elasticity only at temperatures above the glass transition, while the Celcon fibres exhibit this even at temperatures below the glass transition.

These observations indicate the difference in the nature of the amorphouse phase in these two specimens. If the lamellae are connected by a large number of tie chains (taut or loose) and the lamellae and amorphous layers are connected in series, the bulk stress is transmitted through the tie chains and the bulk deformation is augmented by the deformation of individual amorphous layers as depicted in *Figure 20b*. In this case the deformation of lamellae such as bending, hardly contributes to the bulk deformation, since the modulus of the lamella is much higher than that of the amorphous

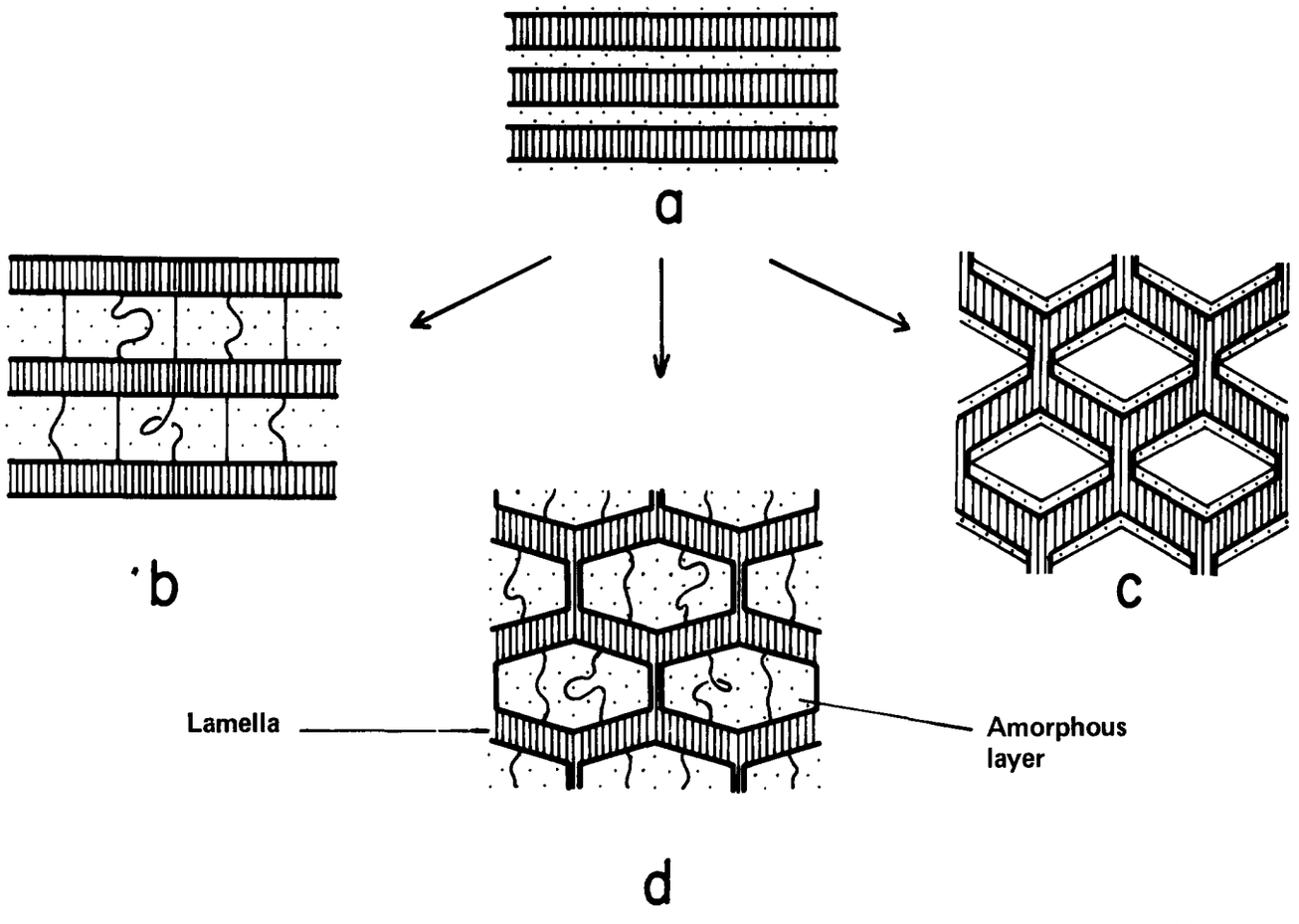

Figure 20 Schematic representation of the deformation behaviour of the lamellae and interlamellar amorphous layers upon stretching the specimens along the ED. (a) undeformed state, (b), (c), and (d) deformed states. In the model (b) the extension of the interlamellar spacing involves the extension of the amorphous layer; orientation of tie chains being the origin of the retractive force, while in the model (c) it involves the lamellar bending or shearing between the tie links; elastic deformation of lamellae being the origin of retractive force and the tie chains being only a minor fraction of the amorphous materials. The model (d) is intermediate between (b) and (c). The extension of the interlamellar spacing involves both lamellar bending or shearing (the deformation of which is smaller than that of (c)) between the tie links or taut tie chains and orientation of the tie chains.

phase. The retractive force which is essentially entropic in origin and the recoverable bulk deformation would then originate from the properties of the tie chains. At temperatures below the glass transition where the micro-brownian motion of chain molecules is frozen, the deformation of the amorphous phase does not involve orientation of tie chains but involves intermolecular deformation, bond stretching, and bending of the valence angle which cannot sustain the large recoverable deformation.

On the other hand, if the lamellae are connected by the tie links (crystal bridges) as pointed out by Clark[13,14] and the tie chains are only a minor fraction of the amorphous materials (thus the amorphous layer is primarily composed of regular and loose loops, cilia, and free chains), the bulk stress is transmitted through the networks of lamellae linked by the crystal bridges. Thus the small deformations of individual lamella (in bending or shearing modes[14]) are cumulative to produce a large bulk deformation of the bulk specimens without exceeding the elastic limit of the lamellae as depicted in *Figure 20c*. Thus the elasticity is energetically driven. In this case the amorphous phase is inactive or makes only a minor contribution to sustain the bulk force and deformation. Thus the long-range elasticity is essentially maintained even at temperatures below the glass transition. This model seems to be relevant to explain the deformation behaviour of typical springy materials such as the elastic Celcon fibres.

The deformation behaviour and the apparent springy properties of the polybutene-1 films may be explained by a model as depicted in *Figure 20d*, i.e., an intermediate between *b* and *c*. The retractive force arises both from those of (loose and taut) tie chains and the lamellar bending or shearing between the tie links or the taut tie chains, a balance of the two factors leading to the energy-driven elasticity (*Figure 19*). The deformation of the interlamellar spacing is a sum of the lamellar deformation and the deformation of the amorphous layer. The deformation of the amorphous layer involves orientation of the tie chains and uniform density-lowering as clarified by the SAXS intensity analyses at temperatures above the glass transition temperature. It involves mechanical yielding and rupture at temperatures below the glass transition.

A quantitative check of the models is best conducted by quantitative studies of crystal and amorphous chain orientations. In particular, the different models would give different amounts of amorphous chain orientation. The assessment of the amorphous chain orientation will be reported in detail in another paper[18].

ACKNOWLEDGEMENTS

This work is partly supported by the grant through the Japan-U.S. Cooperative Research Program, Japan Society for Promotion of Science and National Science Foundation, USA, to which the authors are deeply indebted. The authors are also indebted to the Mitsui Petrochemical Industries, Ltd., Tokyo, Japan, for financial support through a scientific grant.

APPENDIX

The analysis of the SAXS intensity from the deformed specimens

The change of SAXS intensity of the specimens with elongation along the ED may be qualitatively interpreted in terms of a one-dimensional paracrystalline assembly of lamellae, the lamellae being stacked parallel to one another with their chain axes parallel to the ED. If N is the number of lamellae within the assembly, L and a are the average long spacing and thickness of the lamella, respectively, and $f(\underset{\sim}{b})$, $Z(\underset{\sim}{b})$, and $S(\underset{\sim}{b})$ are the particle scattering amplitude, lattice factor and shape amplitude of the assembly, respectively, then the scattered intensity $I(\underset{\sim}{b})$ is given by

$$I(\underset{\sim}{b})/I_e = N[\langle f^2\rangle - \langle f\rangle^2] + \frac{1}{L}\langle f\rangle^2 Z(\underset{\sim}{b}) * |S(\underset{\sim}{b})|^2 \qquad \text{A1}$$

$$Z(\underset{\sim}{b}) = \frac{1}{L}\delta(\underset{\sim}{b}) + Z_1(\underset{\sim}{b}) \qquad \text{A2}$$

$$Z_1(\underset{\sim}{b}) = Re\left\{\frac{1+F(\underset{\sim}{b})}{1-F(\underset{\sim}{b})}\right\} \qquad \text{A3}$$

$$F(\underset{\sim}{b}) = |F(\underset{\sim}{b})|\exp(2\pi ibL) \qquad \text{A4}$$

$$|F(\underset{\sim}{b})| = \exp(-2\pi^2 L^2 g^2 b^2) \qquad \text{A5}$$

where the asterisk* stands for three-dimensional convolution operation, I_e is the Thomson scattering from an electron, and $\underset{\sim}{b}$ is the scattering vector whose magnitude is given by

$$b = (2\sin\theta)/\lambda \qquad \text{A6}$$

and g is the parameter related to the one-dimensional paracrystalline disorder Δ of the lattice spacing from the mean spacing.

$$g = \Delta/L \qquad \text{A7}$$

If the number of lamellae in the assembly is fairly large, so that the function $|S(\underset{\sim}{b})|^2$ changes with b more rapidly than the function $Z_1(\underset{\sim}{b})$, it follows from equations A1 and A2 that

$$I_L(\underset{\sim}{b}) \equiv [I(\underset{\sim}{b}) - I_b(\underset{\sim}{b})]/I_e \simeq N\langle f(\underset{\sim}{b})\rangle^2 Z_1(\underset{\sim}{b}) \qquad \text{A8}$$

where I_b is the background scattering given by

$$I_b(\underset{\sim}{b}) = N[\langle f^2\rangle - \langle f\rangle^2] + \langle f\rangle^2 |S|^2/L^2 \qquad \text{A9}$$

For a lamella of thickness a, the particle amplitude $f(\underset{\sim}{b})$ is given by

$$f(\underset{\sim}{b}) = (\rho_c - \rho_a)\sin(\pi ba)/(\pi b) \qquad \text{A10}$$

where ρ_c and ρ_a are the electron densities of the lamella and amorphous layer, respectively. Neglecting size distribution of a and noting that $a/L = \phi_c$, ϕ_c being volume average crystallinity, and $b_n L = 2(L/\lambda)\sin\theta_n = n$ at scattering angle of the nth order scattering maximum, the intensity of the nth order scattering maximum is given by

$$I_L(b_n) = N(\rho_c - \rho_a)^2 L^2 \frac{\sin^2(\pi n\phi_c)}{(\pi n)^2} Z_1(b_n) \qquad \text{A11}$$

where it follows for small g and n that

$$Z_1(b_n) = \frac{1 + |F(b_n)|}{1 - |F(b_n)|}$$

$$\simeq 2[1 - \exp(-2\pi^2 g^2 n^2)]^{-1} \simeq (\pi^2 g^2 n^2)^{-1} \quad \text{A12}$$

From equations A11 and A12, it follows that

$$I_L(b_n) \cong (\pi n)^{-4} N (L/g)^2 (\rho_c - \rho_a)^2 \sin^2(\pi n \phi_c)$$

$$= (\pi n)^{-4} N (\Delta)^{-2} L^4 (\rho_c - \rho_a)^2 \sin^2(\pi n \phi_c) \quad \text{A13}$$

REFERENCES

1 Tanaka, A., Chang, E. P., Delf, B., Kimura, I. and Stein, R. S. *J. Polym. Sci. (Polym. Phys. Edn)* 1973, **11**, 1891
2 Hashimoto, T., Prud'homme, R. E. and Stein, R. S. *J. Polym. Sci. (Polym. Phys. Edn)* 1973, **11**, 709
3 Kawai, H. *Rheol. Acta* 1975, **14**, 27
4 Onogi, S., Asada, T., Fukui, Y. and Fukisawa, T. *J. Polym. Sci. (A-2)* 1967, **5**, 1067
5 Fukui, Y., Sato, T., Ushirokawa, M., Asada, T. and Onogi, S. *J. Polym. Sci. (A-2)* 1970, **8**, 1195.
6 Hoffman, J. D., Williams, G. and Passaglia, E. *J. Polym. Sci. (C)* 1973, **14**, 173
7 Kyu, T., Yasuda, N., Tabushi, M., Nomura, S. and Kawai, H. *Polym. J.* 1975, **7**, 108
8 Kyu, T., Yasuda, N., Suehiro, S., Nomura, S. and Kawai, H. *Polym. J.* 1976, **8**, 565
9 Suehiro, S., Yamada, T., Inagaki, H. and Kawai, H. *Polym. J.* 1978, **10**, 315
10 Suchiro, S., Yamada, T., Inagaki, H., Kyu, T., Nomura, S. and Kawai, H., submitted to *J. Polym. Sci. (Polym. Phys. Edn)*
11 Suchiro, S., Kyu, T. and Kawai, H., to be submitted
12 Hashimoto, T., Yasuda, N., Suehiro, S., Nomura, S. and Kawai, H. *Polym. Prepr. Am. Chem. Soc., Div. Polym. Chem.* 1976, **17**, 118
13 Garber, C. A. and Clark, E. S. *J. Macromol. Sci (B)* 1970. **4**, 499
14 Clark, E. S. in 'Structure and Properties of Polymer Films', (Eds. R. W. Lenz and R. S. Stein), Plenum Press, New York, 1973
15 Quynn, R. G. and Brody, H. *J. Macromol. Sci. (B)* 1971, **5**. 721
16 Sprague, B. S. *J. Macromol. Sci. (B)* 1973, **8**, 157
17 Cannon, S. L., McKenna, G. B. and Statton, W. O. *J. Polym. Sci. Macromol. Rev.* 1976, **11**, 209
18 Todo, A., Hashimoto, T., Tsukahara, Y. and Kawai, H., to be published
19 Tsukahara, Y., Hashimoto, T. and Kawai, H., to be published
20 See for example, Guinier, A. and Fournet, G. 'Small-Angle Scattering of X-rays', John Wiley & Sons, Inc., New York, 1955, Chap. 3. 4
21 Hashimoto, T., Todo, A., Murakami, Y. and Kawai, H. *J. Polym. Sci (Polym. Phys. Edn)* 1977, **15**, 501
22 Hashimoto, T., Todo, A. and Kawai, H. *Polym. J.* 1978, **10**, 521
23 Hashimoto, T., Nagatoshi, K., Todo, A. and Kawai, H. *Polymer* 1976, **17**, 1063
24 Tanaka, A., Sugimoto, N., Asada, T. and Onogi, S. *Polym. J.* 1975, **7**, 529
25 Stein, R. S., Keedy, D. A., Powers, J. and Plaza, *A. J. Polym. Sci.* 1962, **62**, S89
26 Hosemann, R. and Bagchi, S. N., 'Direct Analysis of Diffraction by Matter', North–Holland Pub. Co., Amsterdam, 1962